Science of the Total Environment 409 (2011) 1219–1228

Contents lists available at ScienceDirect

Science of the Total Environment

journal homepage: www.elsevier.com/locate/scitotenv

Effects of various physicochemical characteristics on the toxicities of ZnO and TiO_2 nanoparticles toward human lung epithelial cells

I-Lun Hsiao, Yuh-Jeen Huang *

Department of Biomedical Engineering and Environmental Sciences, National Tsing-Hua Unversity, 101, Section 2, Kuang-Fu Road, Hsinchu 30013, Taiwan

ARTICLE INFO

Article history:
Received 17 August 2010
Received in revised form 21 December 2010
Accepted 21 December 2010
Available online 20 January 2011

Keywords:
Cytotoxicity
Nanomaterial
Physicochemical characteristics
Human lung epithelial cell (A549)
Occupational health

ABSTRACT

Although novel nanomaterials are being produced and applied in our daily lives at a rapid pace, related health and environmental toxicity assessments are lagging behind. Recent reports have concluded that the physicochemical properties of nanoparticles (NPs) have a crucial influence on their toxicities and should be evaluated during risk assessments. Nevertheless, several controversies exist regarding the biological effects of NP size and surface area. In addition, relatively few reports describe the extents to which the physicochemical properties of NPs influence their toxicity. In this study, we used six self-synthesized and two commercial ZnO and TiO_2 nanomaterials to evaluate the effects of the major physicochemical properties of NPs (size, shape, surface area, phase, and composition) on human lung epithelium cells (A549). We characterized these NPs using transmission electron microscopy, X-ray diffraction, the Brunauer–Emmett–Teller method, and dynamic laser scattering. From methyl thiazolyl tetrazolium (MTT) and Interleukin 8 (IL-8) assays of both rod- and sphere-like ZnO NPs, we found that smaller NPs had greater toxicity than larger ones—a finding that differs from those of previous studies. Furthermore, at a fixed NP size and surface area, we found that the nanorod ZnO particles were more toxic than the corresponding spherical ones, suggesting that both the size and shape of ZnO NPs influence their cytotoxicity. In terms of the effect of the surface area, we found that the contact area between a single NP and a single cell was more important than the total specific surface area of the NP. All of the TiO_2 NP samples exhibited cytotoxicities lower than those of the ZnO NP samples; among the TiO_2 NPs, the cytotoxicity increased in the following order: amorphous>anatase>anatase/rutile; thus, the phase of the NPs can also play an important role under size-, surface area-, and shape-controlled conditions.

1. Introduction

The development of nanotechnology has led to many nanomaterial-containing consumer products appearing in our daily lives. Current statistics suggest that there are more than 1000 products or product lines available worldwide that take advantage of nanotechnology (Rejeski, 2009). Moreover, the presence of nanoparticles (NPs) in these products has also become more widespread. Therefore, it has become necessary to evaluate the safety of NPs in terms of their exposure to occupational workers and consumers.

Because of their small size, NPs have many physicochemical properties that differ from those of their bulk forms (e.g., quantum confinement, surface plasmon resonance, and superparamagnetism effects). Not all of these properties are necessarily beneficial; NPs may also have adverse effects on the environment and human health (Adams et al., 2006; Xia et al., 2007; Aruoja et al., 2009). Recent studies have indicated that the physicochemical characteristics of NPs (e.g., size, shape, surface area, solubility, chemical composition, dispersion factor) play critical roles in determining their biological responses (Oberdorster et al., 2005; Nel et al., 2006; Powers et al., 2006). For example, NPs of smaller size can enter the mitochondria of cells through various pathways, subsequently inducing oxidative stress and cell death via apoptosis (Xia et al., 2007). The relatively larger surface areas of NPs (per volume) can induce greater production of reactive oxygen species (ROS), which then can damage DNA (Karakoti et al., 2006; Hussain et al., 2009). Slightly or completely soluble NPs might release toxic or non-toxic ions that undergo chemical reactions to form ROS (Brunner et al., 2006). The nature of the (charged) functional groups that coat the surfaces of NPs can determine whether or not they enter cells (Zhang and Monteiro-Riviere, 2009). Some authors have attempted to determine how these physicochemical characteristics of NPs affect their biological responses. For instance, for NPs having different abilities to generate reactive species (RS), the phase of the NPs has a greater biological effect than does the surface area (Sayes et al., 2006). In

Abbreviations: NPs, nanoparticles; A549, human lung epithelium cells; MTT, methyl thiazolyl tetrazolium; IL-8, interleukin 8; nano-ZnO, nanozinc oxide; TiO_2, titanium dioxide; TEM, transmission electron microscopy; XRD, X-ray diffraction; BET, Brunauer–Emmett–Teller method; DLS, dynamic laser scattering; ROS, reactive oxygen species; RS, reactive species; EtOH, ethanol; PTFE, polytetrafluoroethylene; EC50, half maximal effective concentration; SSA, specific surface area; FBS, fetal bovine serum; DMEM, Dulbecco's modified Eagle's medium; ELISA, enzyme-linked immunosorbent assay; ZPC, zero point of charge.

* Corresponding author. Tel.: +886 3 5715131x35496; fax: +886 3 5718649.
E-mail address: yjhuang@mx.nthu.edu.tw (Y.-J. Huang).

0048-9697/$ – see front matter © 2010 Elsevier B.V. All rights reserved.
doi:10.1016/j.scitotenv.2010.12.033

addition, many researchers have found that the chemical composition of the NPs is the major factor affecting their cytotoxicity (Gojova et al., 2007).

Although much research has been undertaken in this field, we have yet to reach a consensus on the effects of the various characteristics of NPs, with several disagreements remaining. For example, metal oxide NPs (e.g., Fe_2O_3, Fe_3O_4, TiO_2, ZnO) appear to exhibit no significant size-dependent biological effects toward A549 cells (Lin et al., 2009; Karlsson et al., 2009). When agglomeration of NPs occurs, some reports have suggested that the primary particle size cannot be taken as the practical size for assessing their toxicity (Adams et al., 2006). Indeed, some authors have suggested that the hydrodynamic size determines the cytotoxicity (Kato et al., 2009; Pauluhn, 2009). Moreover, a negation of the biological effects of particle size and surface area has been presented (Warheit et al., 2006). Overall, it is rare for reports to systematically compare physicochemical factors when evaluating NP toxicity. This situation has arisen because many of the samples used in toxicity reports (often obtained commercially) do not satisfy the experimental requirements, and have poor shape, size, and dispersion control during in vitro experiments.

Our aim in this study was to systematically determine the extents to which size, shape, surface area, phase, and composition influence the cytotoxicity of NPs. We used simple synthesis methods (precipitation, solvothermal, sol–gel) to prepare nano-ZnO and nano-TiO_2 (amorphous) materials in different sizes and shapes. We chose to study these materials because (i) they have become important nanomaterials in consumer products and (ii) their synthesis techniques have matured to the stage that we can produce differently sized and shaped NPs on demand.

We evaluated the toxicities of spherical, sphere-like, and rod-like ZnO having well-controlled sizes and surface areas. Furthermore, we used amorphous, anatase, and anatase/rutile TiO_2 NPs to determine the effect of the phase on toxicity. All of the NPs used in this study were characterized in terms of size, shape, phase, surface area, and dispersion, using transmission electron microscopy (TEM), X-ray diffraction (XRD), Brunauer–Emmett–Teller (BET), and dynamic light scattering (DLS) techniques, prior to applying the NPs to exposure tests. For cytotoxicity assessments, we chose human lung epithelial cells (A549) as the target. The cell morphology, metabolic activity, and the production of inflammation mediators were evaluated using a digital image system, 3-(4,5-dimethylthiazol-2-yl)-2,5-diphenyltetrazolium bromide (MTT) assays (Mossman, 1983), and interleukin 8 (IL-8) assays (Beutler et al., 1985), respectively. Herein, we compare the toxic tendencies of the various characteristics (size, shape, surface area, phase) of the TiO_2 and ZnO NPs toward A549. We hope that our findings will provide more clear and confident information regarding the effects of the physicochemical characteristics of NPs on in vitro toxicity, and that our results can be used to prejudge the main sources of cytotoxicity when cells become exposed to environmental NPs.

2. Materials and methods

2.1. Chemicals

Anatase-phase TiO_2 NPs (ST-21) were purchased from Ishihara Sangyo Kaisha (Japan); the anatase/rutile mixture of TiO_2 NPs was obtained from Degussa (Germany). Zinc acetate dihydrate [$Zn(CH_3COO)_2 \cdot 2H_2O$, reagent grade], and absolute ethanol (EtOH, 99.5%) were purchased from Sigma–Aldrich (St. Louis, MO); sodium hydroxide (NaOH) pellets (99%) and ammonium hydroxide (28%) were obtained from J. T. Baker (Phillipsburg, NJ); lithium hydroxide (LiOH, 98%) and tetrabutyl orthotitanate (TBOT, 98%) were purchased from E. Merck (Darmstadt, Germany). All aqueous solutions for chemical and biological experiments were prepared using 18.2 MΩ cm ultrapure deionized water obtained from a Millipore Simplicity system (Millipore, S.A.S.).

2.2. NP preparation

2.2.1. Preparation of nanorod ZnO

Nanorod ZnO NPs were prepared using a simple precipitation method (Cao et al., 2006). Zinc acetate dihydrate was dissolved in absolute EtOH (200 mL) and then NaOH pellets were added; the mixture was stirred for 1.5 h to dissolve the solutes at room temperature. The molar ratio of Zn^{2+} and OH^- was controlled at 1:25. The solution was then placed in the dark for 1 or 14 days at room temperature. The deposits in the solution were collected through centrifugation (1900 g, 10 min), washed sequentially with water and EtOH several times, and then dried in a vacuum oven at room temperature overnight.

2.2.2. Preparation of nanosphere ZnO

Nanosphere ZnO NPs having a primary particle size of less than 10 nm were prepared using a low-temperature precipitation method (Ge et al., 2007). Zinc acetate dihydrate (0.88 g) was dissolved and heated in absolute EtOH (80 mL) at 70 °C for 20 min. Separately, LiOH (0.23 g) was added to absolute EtOH (80 mL) and stirred vigorously for 30 min at room temperature. The alkaline solution was added dropwise over 1 h into the Zn^{2+}-containing solution at 0 °C under strong magnetic stirring. The mixture was then sonicated for 5 min; the solid products were separated by centrifugation, washed sequentially with EtOH and water, and then dried under vacuum at room temperature overnight.

2.2.3. Preparation of sphere-like nano-ZnO

Sphere-like nano-ZnO NPs with good dispersibility were prepared using a solvothermal process (Du et al., 2004). Zinc acetate dihydrate (2.5 g) was added to absolute EtOH (30 mL) and then sonicated for 30 min. The mixture was transferred into a 300-mL Teflon-lined autoclave and thermostated in an oven at 120 or 180 °C for 24 h. The white product was filtered off through a 0.1-μm PTFE membrane filter, washed five times with EtOH, and then dried in a vacuum oven at room temperature overnight.

2.2.4. Preparation of amorphous TiO_2 NPs

Amorphous-phase TiO_2 NPs were synthesized using a sol–gel method (Liao et al., 2006). TBOT (0.1 mL) was added to deionized water (7.5 mL) and sonicated for 5–10 min; the resulting solution was added dropwise (2 mL min^{-1}), using a microtubing pump (MP-1000, EYELA, Tokyo), to a mixture of ammonium hydroxide (28%, 9 mL) and absolute EtOH (80 mL) under vigorous stirring at room temperature. After 24 h, the precipitate was collected through centrifugation, washed several times with absolute EtOH and water, and then dried under vacuum at 50 °C for 24 h.

2.3. Characterization of NPs

2.3.1. Sizes, shapes, surface area, and phase

The particle size distributions and morphology of the prepared NPs were analyzed using a TECNAI 20 transmission electron microscope (Philips, Netherlands). Prior to measurement, the particles were dispersed in absolute EtOH (300 μg mL^{-1}). After 20 min of bath sonication, aliquots (5 μL) of the suspensions were deposited on 200-mesh carbon-formvar copper grids and then the solvents were evaporated in a vacuum oven for 1 h. The specific surface area (SSA) of the NPs was determined, in terms of the N_2 adsorption on the powder, using the BET method (Brunauer et al., 1938). The measurement was performed using a volumetric adsorption apparatus (NOVA Surface Area Analyzer Station A, USA); the vacuum system was operated at a liquid nitrogen temperature (77.3 K) after degassing for 3 h at 200 °C.

The crystalline structures of the ZnO and TiO_2 NPs were analyzed using an MXP18 X-ray diffractometer (MAC Science, Japan). The

analysis was performed in the 2θ range from 25 to 75° using copper-$K_{\alpha 1}$ ($\lambda = 1.54056$ Å) radiation, with a tube potential of 20 kV, a current of 20 mA, and a scan rate of 3° min^{-1}. The Debye–Scherrer formula was used to calculate the particle grain sizes (Klug and Alexander, 1954):

$$d = \frac{K\lambda}{\beta\cos\theta} \quad (1)$$

where d is the average size of the particle, K is a constant (0.9), λ is the X-ray wavelength, β is the full-width at half-maximum (in radians), and θ is the maximum angle of diffraction.

2.3.2. Agglomeration state and surface charge

The hydrodynamic size and surface charge of the NPs in water and cell culture media were monitored using a Zetasizer Nano ZS apparatus (Malvern Instruments, UK). The particle size was determined using DLS. The relationship between the size of a particle and its speed, due to Brownian motion, is defined by the Stokes–Einstein equation:

$$d_p = \kappa T / 3\pi\mu D \quad (2)$$

where d_p is the hydrodynamic diameter (defined as the diameter of a sphere that has the same diffusion coefficient), κ is the Boltzmann constant (J K^{-1}), T is the absolute temperature (K), μ is the viscosity of the medium (kg m^{-1} s^{-1}), and D is the average diffusion coefficient (m^2 s^{-1}), which can be evaluated by illuminating the particles with a laser and analyzing the intensity fluctuations in the scattered light.

The zeta potentials were measured by determining the electrophoretic mobility and then applying the Henry equation. The electrophoretic mobility of each set of particles was obtained by performing an electrophoresis experiment (applying an electric field across the dispersion) and measuring the velocity of the particles using laser Doppler velocimetry (LDV). According to the Henry equation,

$$Ue = 2\varepsilon z f(ka) / 3\eta \quad (3)$$

where Ue is electrophoretic mobility (m^2 V^{-1} s^{-1}), z is the zeta potential (V), ε is the dielectric constant of the medium, η is the viscosity, and $f(ka)$ is a constant (1.5, known as the Smoluchowski approximation), the zeta potential can be calculated if Ue can be determined by detecting the frequently shift of scattered light from the moving particles (Malvern Instruments, Ltd, 2004).

For measurement of the secondary size, the NPs were dispersed (at 200 μg mL^{-1}) in water and Dulbecco's modified Eagle's medium (DMEM High Glucose, w/L-Glutamine, Biosera, UK). To decrease the degree of agglomeration, the dispersions were sonicated in an ice bath using an ultrasonic probe (8 W, 22 kHz) for 5 min prior to measurement. The time-dependent variations in the degrees of NP agglomeration were measured over 48 h for two nanorod and two sphere-like ZnO NPs.

2.4. Cell culture and cytotoxicity assays

The human lung carcinoma epithelial cell line (A549) was purchased from Bioresource Collection and Research Center (BCRC-60074, Taiwan). The cell line was cultured in DMEM supplemented with 10% fetal bovine serum (FBS) and 1% penicillin, streptomycin, and amphotericin, and cultivated in T25 flasks at 37 °C in a humidified atmosphere of 5% CO_2/95% air.

2.4.1. Preparation of stock solution

Before the powder samples were applied to the in vitro systems, each was suspended in dimethyl sulfoxide (DMSO, Sterile, Sigma–Aldrich) at a concentration of 20 mg mL^{-1}. All stock solutions were dispersed using a 5-W probe sonicator (Ultrasonic Cell Disruptor, Misonix, USA) for 90s in an ice bath.

2.4.2. Sample treatment

Stock solutions of the nano-powders were diluted to concentrations ranging from 50 to 1.56 μg mL^{-1} in serum-free DMEM. To stabilize the suspensions, the NP-containing media were then sonicated using a 400-W/40-kHz ultrasonic cleaner (DC-400H, Delta, Taiwan). For assessments of the morphology and cytotoxicity, the cells (4×10^4 cells mL^{-1}) were seeded in 96-well plates (BD Falcon, USA). To evaluate the cell number, a standard curve for the MTT assay was performed by seeding cells (from 1.56×10^3 to 1×10^5 cells mL^{-1}) in the 96 wells. After 24 h of cell attachment, the cells were exposed to the diluted NP solutions for 12, 24, or 72 h. Three replicate wells per microplate were used for each control and test concentration, respectively.

2.4.3. Cell morphology

The cell morphology was assessed following exposure to the NPs using a Zoomkop EZ-20I inverted optical microscope (Leader Scientific, Taiwan) coupled to an Olympus SP-350 digital compact camera system (magnification: ×100).

2.4.4. MTT assay

After exposure, the dosage solutions were aspirated to another plastic plate and stored at 4 °C for subsequent IL-8 analysis. The cells were rinsed once with phosphate-buffered saline (PBS, 1×) and then fresh medium (with 10% FBS; 200 μL) was added to each well. Next, MTT (5 mg mL^{-1}, 20 μL; Aldrich) was added to each well and then the plates were incubated for 3 h at 37 °C in a 5% CO_2 incubator. After incubation, the medium/MTT solution was discarded and DMSO (200 μL) was added to each well. Finally, the absorbance was measured at 570 nm using a VersaMax tunable microplate reader (Molecular Devices, USA). The relative cell activity (%) of the NP-dosed wells, with respect to that of the non-exposed wells, was calculated using the expression [cell number of testing samples]/[cell number of control]×100.

2.4.5. Production of IL-8

The sandwich ELISA protocol was used for the human IL-8 assay (Human IL-8 ELISA Kit and buffer, PeproTech, USA). The capture antibody (0.5 μg mL^{-1}, 100 μL) was added to each 96-well ELISA plate (Maxisorp, Nunc, NY) and then incubated overnight at room temperature. Next, blocking solution (200 μL) was added to each well, with incubation for 1 h. The sample (100 μL) and the IL-8 standard (16–2000 pg mL^{-1}) were then added to each well, with incubation for 2 h. The detection antibody (0.25 μg mL^{-1}, 100 μL) was then added, with incubation for 2 h. Diluted adivin/HRP conjugate (1:2000) solution (100 μL) was then added to each well, with incubation for 30 min. Between each of these steps, the solutions in each well were aspirated and washed four times with washing buffer. Next, the color reaction solution [3,3′,5,5′-tetramethylbenzidine (TMB), 100 μL] was added to each well. After sufficient color development (20 min at room temperature), the stop solution (2 M H_2SO_4, 50 μL) was added to each well. Finally, the absorbance was measured at 450 nm using a tunable microplate reader.

2.4.6. Statistics

Through regression analysis, the standard curve for the MTT assay was accepted only when the value of R^2 of the logarithm curve reached 0.99. The effects of the various NPs on the cell cultures were analyzed statistically, to a significance level p of less than 0.05, using a one-tailed Student's t-test. The EC50 values determined from the dose–response curves were calculated using GraphPad Prism 5.02 (GraphPad Software, San Diego, USA) and the equation:

$$y = Bottom + (Top–Bottom) / \left(1 + 10^{x- logEC50}\right) \quad (4)$$

3. Results and discussion

3.1. Physicochemical characterization (TEM, XRD, BET)

We recorded TEM images to determine the sizes and morphologies of the synthesized and commercial NPs (Fig. 1). The rod-shaped nano-ZnO NPs that we prepared using the precipitation method over 1 and 14 days had similar diameters (ca. 5 nm), but different lengths, within the ranges 5–16 and 16–48 nm, respectively (Fig. 1a and b). We prepared the spherical nano-ZnO NPs having average diameters of less than 10 nm through low-temperature precipitation; their primary particle size was 5–10 nm (Fig. 1c). These particles all underwent serious degrees of aggregation (ca. 500 nm) in DI water (Table 1). Performing the solvothermal syntheses without adding any alkaline agents led to lower degrees of aggregation of the nano-ZnO NPs and produced sphere-like NPs in the size ranges 36–68 and 50–122 nm (from the 120 and 180 °C syntheses, respectively; Fig. 1d and e). TiO_2-A, which we synthesized using a sol–gel method, had a less-uniform spherical morphology, with a primary size distribution of 90–160 nm; it had a different size distribution and morphology relative to those of the ST-21 and P25 TiO_2 NPs (Fig. 1f–h).

The XRD patterns of the ZnO products revealed all characteristic peaks of bulk ZnO, suggesting that they possessed hexagonal wurtzite structures (Fig. 2a–e). The synthesized TiO_2 NPs featured no characteristic peaks, confirming their amorphous phase (Fig. 2f). Notably, we observed no impure crystalline phases for any of our materials (Fig. 2a–f). The half-height-to-width ratios of the (0 0 2) and (1 0 1) peaks confirmed the anisotropic rod shapes of the ZnO NPs (Fig. 2a and b); the grain sizes of the two nanorod ZnO NPs were 6×8 nm and 7×19 nm, respectively, as calculated using the Debye–Scherrer formula. Table 1 lists the grain sizes of the other nano-ZnO NPs; we use a nomenclature involving the particle composition, a letter representing its shape or phase (R, rod; S, spherical or sphere-like; A, amorphous), and a number representing its grain size.

The SSAs of the ZnO and TiO_2 NPs, measured using the BET method, were 88 and 37 $m^2\ g^{-1}$ for ZnO-R8 and ZnO-R19, respectively, 90 $m^2\ g^{-1}$ for ZnO-S6, 15 and 7 $m^2\ g^{-1}$ for ZnO-S25 and ZnO-S38, respectively, and 38 $m^2\ g^{-1}$ for TiO_2-A. Table 1 lists the SSAs and phases of the reported P25 and ST-21 NPs (Sun and Smirniotis, 2003; Ito et al., 2007).

3.2. Agglomeration state and surface charge

When these NPs are suspended in aqueous systems, aggregation usually occurs. Thus, the secondary size (also known as the hydrodynamic size) might also be a factor affecting the particles' cytotoxicities. Table 1 lists the secondary size and surface charge of the ZnO and TiO_2 NPs in water and DMEM. For the ZnO NPs, different degrees of aggregation occurred when using the different preparation methods. ZnO-R8 (914 nm in DMEM), ZnO-R19 (1093 nm in DMEM), and ZnO-S6 (795 nm in DMEM), which we fabricated using the precipitation method, exhibited greater degrees of agglomeration than ZnO-S25 (640 nm in DMEM) and ZnO-S38 (687 nm in DMEM), which we fabricated using the solvothermal method, even through the former three NPs had smaller primary particle sizes. Nevertheless, regardless of whether we used the precipitation or solvothermal method, the smaller-sized ZnO particles aggregated to smaller secondary sizes than the larger NPs. For the TiO_2 NPs, the average sizes of the ST-21 and P25 NPs in water were 180 and 211 nm, respectively; they formed larger agglomerates in DMEM (1843 and 1814 nm, respectively). Although TiO_2-A exhibited lower stability in water (661 nm), it featured a smaller secondary size in DMEM (1054 nm). The net surface charges of the ZnO NPs were all positive in water, but those of the TiO_2 NPs were all negative (Table 1).

Fig. 3 presents the flowchart that we followed to investigate the effects of the physicochemical properties on the toxicities of the NPs. Because of their well-controlled primary size and secondary size, here we used the ZnO-R8, ZnO-R19, ZnO-S25, and ZnO-S38 NPs as examples to discuss the effects of the size and surface area on the cytotoxicity. Because ZnO-S6 and ZnO-R8 had similar surface areas and sizes, we used them to study the effect of the NP shape. We discuss the effects of phase on the cytotoxicity based on the data from all of the TiO_2 NPs. Combining the toxicity results obtained from the ZnO and TiO_2 NPs allowed us to compare the effects of chemical composition on nanotoxicity. We evaluated the toxicities of all of the

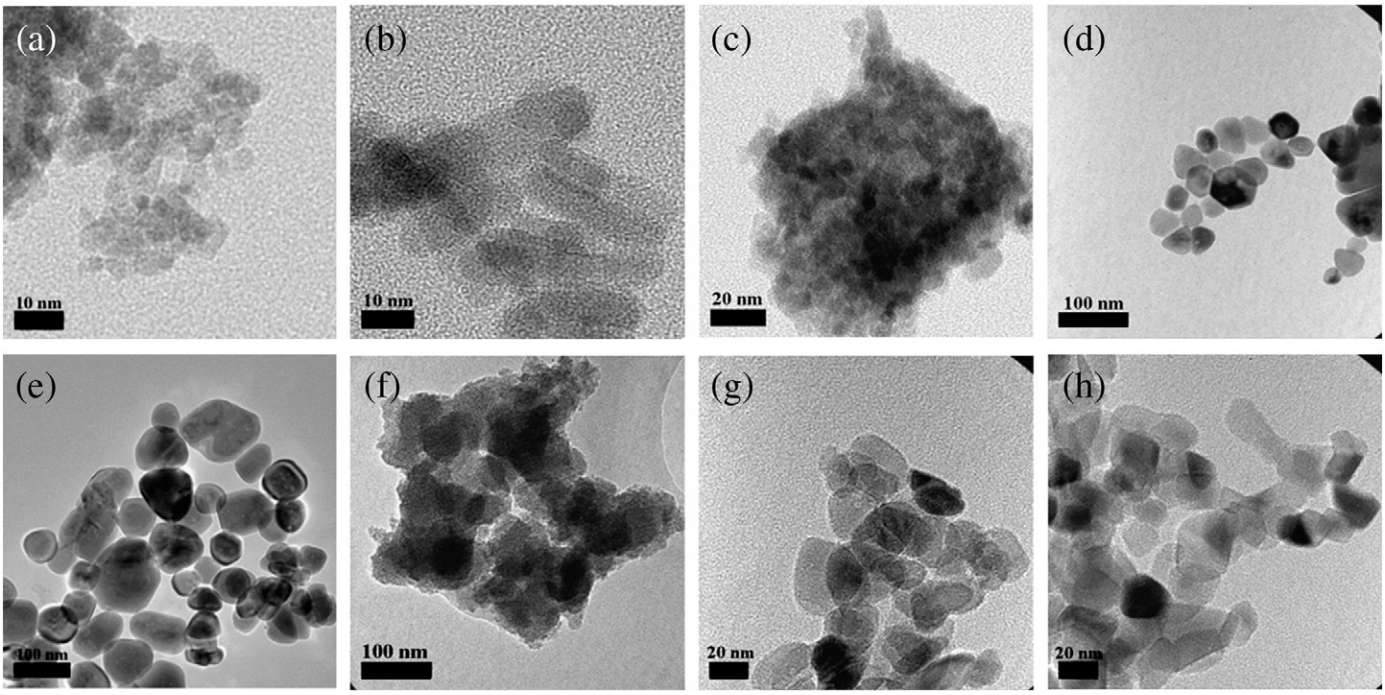

Fig. 1. TEM images of ZnO and TiO_2 NPs. (a) ZnO-R8, (b) ZnO-R19, (c) ZnO-S6, (d) ZnO-S25, (e) ZnO-S38, (f) TiO_2-A, (g) Ishihara ST-21, and (h) Degussa P25.

Table 1
Characterization data of nano-ZnO and nano-TiO_2 particles.

Sample	Size distribution[a] (nm)	Average grain size[b] (nm)	BET surface area (m^2 g^{-1})	Hydrodynamic diameter (DLS) (nm) and PDI				Zeta potential[c] (mV)
				DI water		DMEM		
				DLS	PDI	DLS	PDI	
Synthesized nanopowder								
ZnO-R8	5–16	D×L[d] = 6×8	88	481	0.23	914	0.38	29.8
ZnO-R19	16–48	D×L = 7×19	37	593	0.37	1093	0.44	21.6
ZnO-S6	5–10	6	90	505	0.34	795	0.53	27.4
ZnO-S25	36–68	25	15	183	0.30	640	0.26	29.4
ZnO-S38	50–122	38	7	198	0.24	687	0.33	31.3
TiO_2-A	90–160	Amorphous	38	661	0.30	1054	0.23	−40.8
Commercial nanopowder								
Ishihara ST-21	22–38	Anatase (100%)20 nm / Anatase (80%)21 nm	69	180	0.15	1843	0.21	−30.8
Degussa P25	18–53	Rutile (20%) 50 nm	66	211	0.28	1814	0.27	−35.5

[a] Size distributions of NPs were determined from TEM images.
[b] Grain sizes of NPs were calculated using the Debye–Scherrer formula.
[c] Zeta potentials of the NPs were measured in deionized water at 25 °C.
[d] "D," nanorod diameter; "L," nanorod length.

NPs using cell morphology, MTT, and IL-8 assays with exposure times of 12, 24, and 72 h.

3.3. Size and surface area effect

To determine the effects of the size and surface area of the ZnO NPs on their cytotoxicity, we monitored the behavior of rod and spherical NPs of various sizes. Before performing the toxicological experiments, we used a Zetasizer to measure the variations in particle size in DMEM with respect to exposure time. Each of the ZnO NPs displayed an increased hydrodynamic size during the initial 12 h, but decreased thereafter. Furthermore, the sphere-like NPs provided more stable size (ca. 2300 nm, 12 h) than the rod-like NPs (ca. 3500 nm, 12 h), even though the former had larger primary size. Irrespective of the shape of the NPs, smaller particles aggregated into smaller secondary particles during the exposure period (Fig. 4).

In terms of cell morphology, the typically elongated A549 cells formed abnormally spherical shapes after exposure to the ZnO nanorods (Fig. 5b and c), revealing that the cells were either damaged or dead. The aggregation that we observed for the NPs in DMEM was also evident in the cells, with ZnO-R19 providing a larger secondary size, consistent with our Zetasizer result. More ZnO-R8 particles were located in the periphery of the cell membrane and internalized into the cytoplasm, thereby potentially inducing greater cytotoxicity.

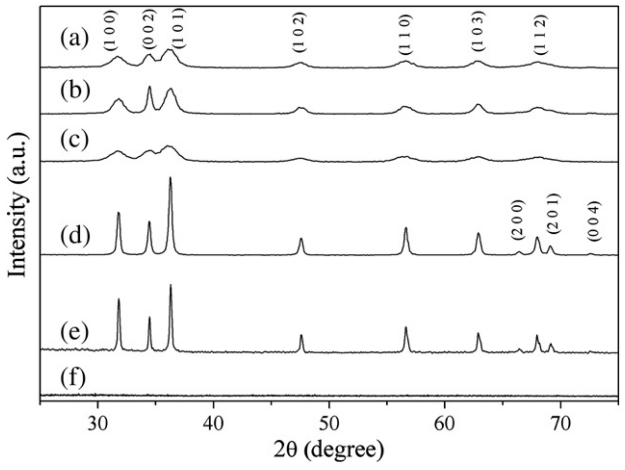

Fig. 2. XRD patterns of synthesized NPs. (a) ZnO-R8, (b) ZnO-R19, (c) ZnO-S6, (d) ZnO-S25, (e) ZnO-S38, and (f) TiO_2-A.

Mitochondria activity (MTT) and IL-8 assays have been used previously to screen different levels of oxidative stress, from severe cytotoxicity to slight inflammation (Nel et al., 2006). Fig. 6 presents the time- and dose-responses of the rod- and sphere-like nano-ZnO toward A549 cells. The time-dependent cytotoxicity data revealed that all of the ZnO NPs not only had inhibitory effects but also caused death to cells (Fig. 6a and c). The dose–response curves of the two R8 samples display steeper declines in cell viability in each time-course experiment (Fig. 6a); the EC_{50} values of ZnO-R8 and ZnO-R19 after 72-h exposure were 4.6 and 8.2 μg mL^{-1}, respectively. We observed the same behavior for the sphere-like NPs (Fig. 6c); the EC_{50} values of ZnO-S25 and ZnO-S38 after 72-h exposure were 10.7 and 11.9 μg mL^{-1}, respectively. Furthermore, production of inflammatory factor IL-8 in the presence of the rod- and sphere-like NPs was enhanced for the smaller-sized NPs. In addition, we observed that more than twice the amount of IL-8 was released from each A549 cell treated with the sphere-like NPs than with the rod-like NPs.

Regardless of shape, we observed size-dependent cytotoxicity for the nano-ZnO NPs in the MTT and IL-8 assays. Many researchers have noted the effect of size on the cytotoxicity of some, but not all, NPs (Yamamoto et al., 2004; Carlson et al., 2008; Karlsson et al., 2009; Napierska et al., 2009). Nano-scale ZnO particles were found to be more toxic toward osteoblast cancer cells and to exhibit greater antibacterial activity than were their corresponding micro-sized ZnO particles (Nair et al., 2008). Notably, however, the size-dependent toxicity of nano-ZnO particles was not observed at levels of exposure of less than 24 ppm (Lin et al., 2009; Deng et al., 2009). The authors of those studies provided two reasons for the absence of a size-dependent effect. The first is that the NPs, regardless of their size, formed aggregates of similar hydrodynamic size and that these aggregates had similar cytotoxicities (Deng et al., 2009). The researchers typically used commercial powder samples, which comprised rod-like and irregularly shaped particles; the complex aggregation states formed from differently shaped particles might result in similarly sized aggregates. To eliminate this obstacle, in this present study we used synthesized nano-ZnO NPs that had well-controlled shapes and sizes. The second explanation is related to the role played by dissolved zinc ions formed from the ZnO particles (Xia et al., 2008; Deng et al., 2009; Sharma et al., 2009). The maximum zinc ion release in serum-containing DMEM is ca. 18.2 ppm (Xia et al., 2008); in our present study, we used serum-free medium in which the dissolution of zinc ions is lower (5.8–7.2 ppm, Table S1). These conditions should result in particle-to-cell interactions dominating, even at low concentrations. For these two reasons, we expected that,

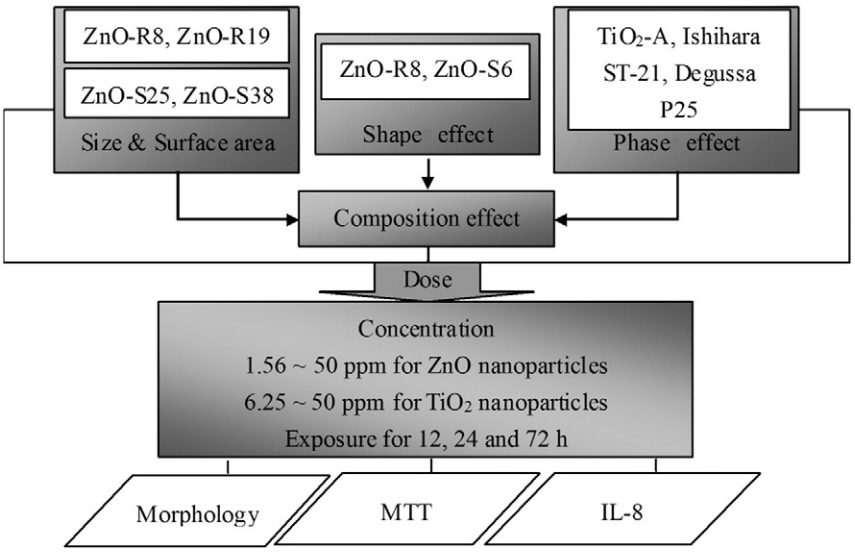

Fig. 3. Flowchart of the toxicological study.

even if the size variations of the NPs were slight and the exposure concentrations were low, we would observe a size-dependent toxicity effect in this study.

Hydrodynamic size is a good tool for assessing the cytotoxicity of NPs because aggregation of NPs always occurs in cell culture solutions [e.g., DMEM, RPMI, F-12; (Murdock et al., 2008; Allouni et al., 2009)]. The primary size of NPs might, however, still contribute to the toxicity, as noted in some reports (Braydich-Stolle et al., 2009). In this case, ZnO NPs having smaller primary sizes could form relatively small secondary aggregates that cause greater cytotoxicity. In addition, we found that the sphere-like nano-ZnO NPs induced more potential IL-8 than the nanorod ZnO NPs, presumably because of the lower degree of aggregation of the sphere-like NPs. Therefore, both the primary size and the secondary size might determine the cytotoxicity of a nanomaterial.

Regardless of their shape, ZnO NPs having larger SSAs might provoke more serious cytotoxicity (Fig. 7a and b). Although we noted above that smaller NPs exhibited higher toxicities, the surface area effect on A549 cells revealed a different phenomenon: for the same surface area, the larger-sized NP caused greater cell death.

In general, smaller particles have larger SSAs, leading to greater contact with cells and more potential damage (Karakoti et al., 2006).

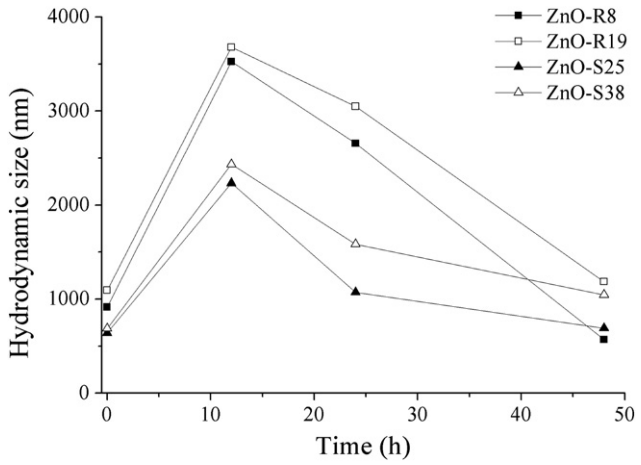

Fig. 4. Time evaluation of the sizes of ZnO NPs in DMEM over a period of 48 h.

The surface area parameter has also been presented as a suitable dose metric for inhalation exposure (Sager et al., 2008). Nevertheless, compared with the effects of the composition and phase, the surface area might not be as important a parameter affecting cytotoxicity (Sayes et al., 2006; Gojova et al., 2007). In our present study, we found that although they have the same surface area, ZnO-R19 and ZnO-S38 displayed more serious toxicity than ZnO-R8 and ZnO-S25. These findings revealed to us that the "real" surface area of the NPs contacting the cells determines the toxicity. As a corollary, when measuring exposure to NPs, we should express the concentration of particles as a number, not as a mass dosage. A single NP having a larger surface area should cause more cell damage than smaller surface area ones.

3.4. Shape effect

We used ZnO-R8 and ZnO-S6 to determine the effect of shape on cytotoxicity because their primary sizes, secondary sizes in water and DMEM, crystallinities, and surface areas were all similar. Fig. 8a reveals that the nanorods and nanospheres had similar cytotoxicities after exposure for 12 h; after 24 h, however, the nanorod ZnO NPs were more toxic than the nanosphere ZnO NPs, with values of EC_{50} for ZnO-R8 and ZnO-S6 of 8.5 and 12.1 μg mL^{-1}, respectively. The IL-8 test also revealed significantly different levels of inflammation at 3.13 μg mL^{-1} (Fig. 8b). Overall, the shape of the nano-ZnO NPs appeared to dominate the toxicity when the size and surface area were controlled.

Anisotropic particles (e.g., fibers) can cause greater long-term effects, such as fibrosis and lung cancer (Peto et al., 1977). Previous studies have revealed that carbon nanomaterials—for example, single-walled carbon nanotubes (SWCNTs)—are more toxic than carbon black at the same mass dosage (Lam et al., 2004). CNTs also cause more DNA damage and genotoxicity than the spherical ZnO and TiO_2 NPs (Yang et al., 2009). Dendritic TiO_2 NPs induce the highest degree of cytotoxicity toward the mouse macrophage cell line (J774A.1), followed by spindle- and sphere-shaped NPs (Yamamoto et al., 2004). A comparison of whisker-shaped SiC and its particulate form revealed that only the former exhibited toxicity toward hamster lung fibroblast cells (V79-4; Birchall et al., 1988). There are, however, two problems when estimating shape-caused cytotoxicity. One is cell sensitivity and phagocytic ability, which sometimes might make it difficult to detect such a difference. The other is that the interaction forces of lengthwise-oriented NPs increase proportionally to their lengths

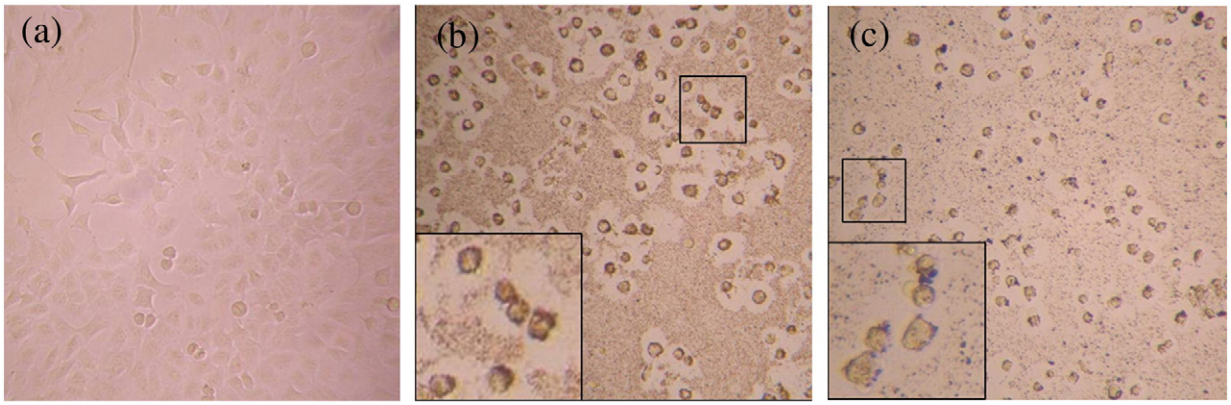

Fig. 5. Morphologies of A549 cells exposed to nanorod ZnO for 24 h; magnification: ×100. (a) Control, (b) ZnO-R8 (50 μg mL^{-1}), and (c) ZnO-R19 (50 μg mL^{-1}). Insets to b and c: higher magnification images.

(Brown et al., 2007). Therefore, the van der Waals forces of rod-shaped NPs are larger than those of spherical ones. In this present study, we found that ZnO-R8, which had a less-asymmetrically-oriented length, formed aggregates of similar size as those of ZnO-S6 in both water and DMEM. In addition, serum-free exposure increased the cell phagocytic ability, thereby revealing the different toxicities of the rod- and sphere-shaped NPs. The effect of the shape of an NP on its cytotoxicity can be attributed to the number of edges that induce serious oxidative stress (Yamamoto et al., 2004), but additional evidence will be required to support this hypothesis.

3.5. Phase and composition effect

We used TiO_2 NPs of various phases to determine the effect of a particle's phase on A549 cells. The cytotoxicity of the TiO_2 samples decreased in the order TiO_2-A>ST-21>P25 after exposure for both 12

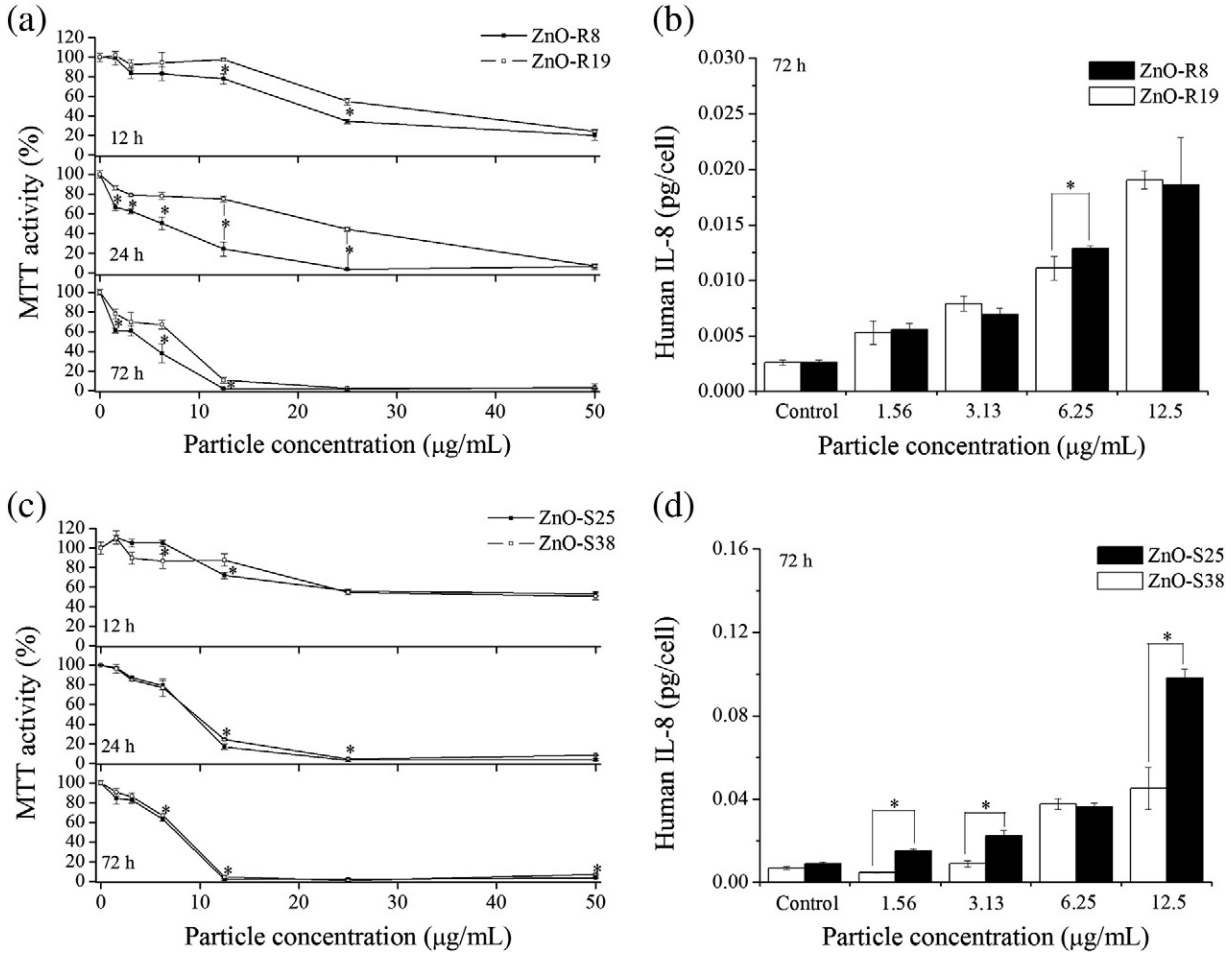

Fig. 6. Size-dependent responses for the cytotoxicity of ZnO NPs. (a) Time–response curves for the MTT activity of ZnO nanorods. (b) IL-8 production of ZnO nanorods during 72-h exposure. (c) Time–response curves for the MTT activity of sphere-like nano-ZnO. (d) IL-8 production of sphere-like nano-ZnO during 72-h exposure. Asterisks (*) denote, at the same mass concentration, groups that have significant differences toward other groups at a 95% confidence level.

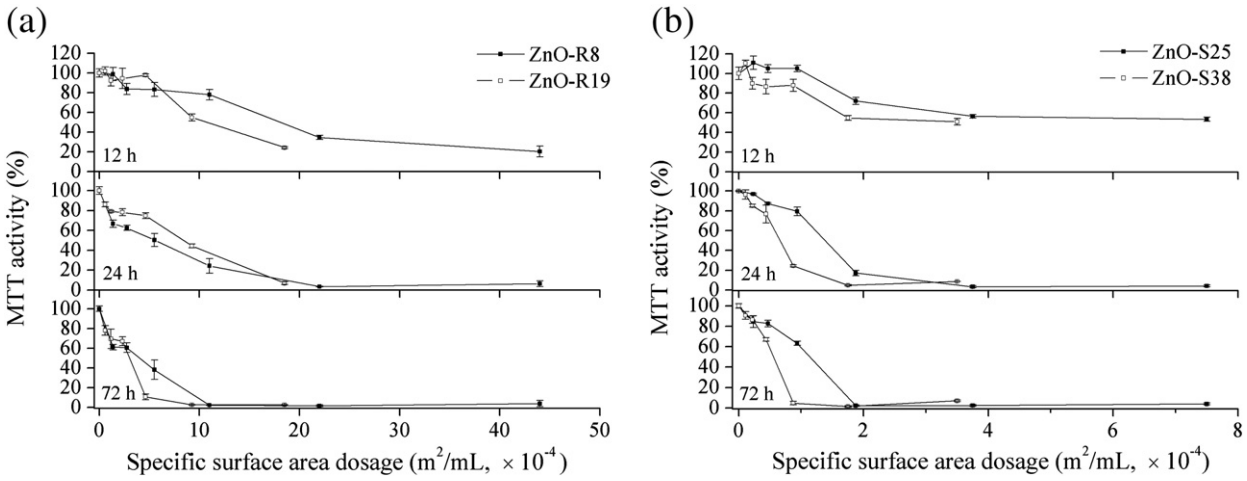

Fig. 7. Exposure of A549 cells to (a) ZnO nanorods and (b) sphere-like nano-ZnO using the particles' SSAs as dosimetry.

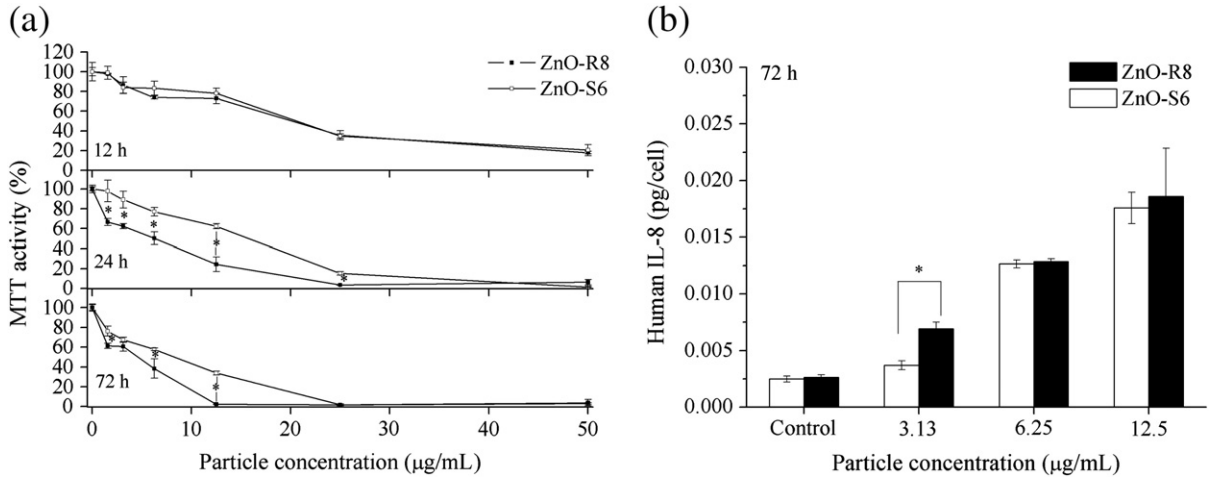

Fig. 8. Shape-dependent responses for the cytotoxicity of ZnO NPs. (a) Time–response curves for the MTT activities of ZnO nanorods and nanospheres. (b) IL-8 production induced after exposure to the ZnO nanorods and nanospheres for 72 h. Asterisks (*) denote, at the same mass concentration, groups that have significant differences to other groups at a 95% confidence level.

and 72 h (Fig. 9a). The amorphous TiO_2 and ST-21 NPs exhibited greater potential to induce more pro-inflammatory factor in human cells than did the P25 NPs (Fig. 9b). Although the ST-21 and P25 NPs had a similar surface area (ca. 68 $m^2\ g^{-1}$), size (ca. 20 nm), and shape (spherical), they induced different toxicity responses, confirming that the phase of a TiO_2 NP affects its cytotoxicity. We observed significant

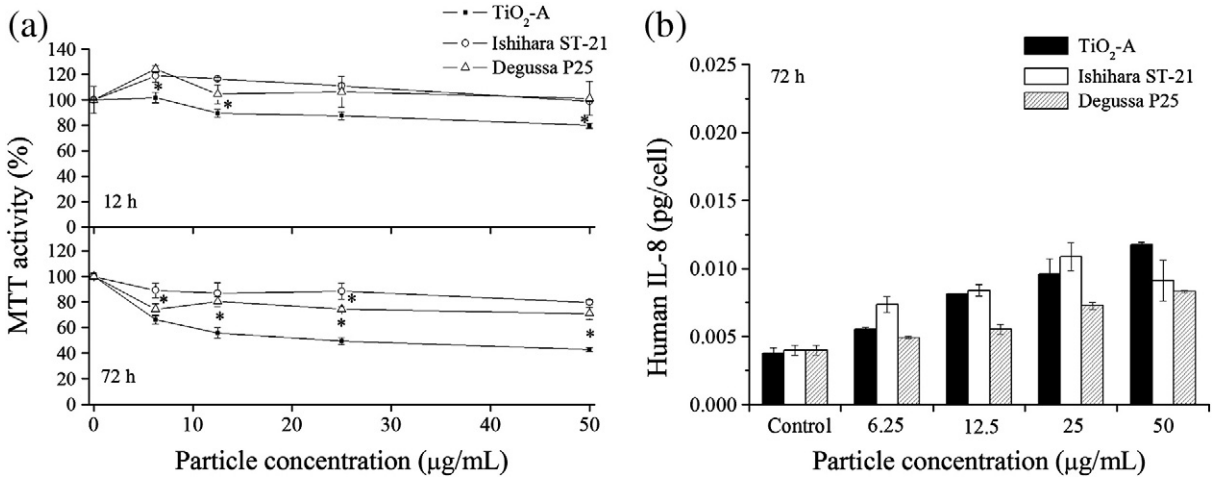

Fig. 9. Phase-dependent responses for the cytotoxicity of ZnO NPs. (a) Time–response curves for the MTT activities of amorphous, anatase, and anatase/rutile mixture nano-TiO_2 NPs. (b) IL-8 production induced after exposure to TiO_2 NPs for 72 h. Asterisks (*) denote, at the same mass concentration, groups that have significant differences to other groups at a 95% confidence level.

toxicity differences for the ZnO and TiO_2 NPs. Even for the most-toxic TiO_2 NPs, namely the amorphous TiO_2 NPs, the cell viability remained absolutely higher than and the chemokine release approximately half that of the ZnO samples after exposure for 72 h.

According to some reports, the crystal structure of an NP influences its cytotoxicity, with the anatase form of TiO_2 being slightly more toxic than the rutile form (Sayes et al., 2006; Braydich-Stolle et al., 2009); thus, we would have predicted greater toxicity for the ST-21 (anatase). Few studies, however, have noted whether amorphous-phase TiO_2 has any toxicity (Jiang et al., 2008). Our results revealed that only amorphous-phase TiO_2 NPs induced 50% cell death after exposure for up to 72 h at concentrations of up to 25 μg mL^{-1} (Fig. 9a). Unfortunately, this amorphous TiO_2 did not exhibit a similar size to ST-21 and P25 NPs; therefore, our results could not be explained completely in terms of a phase-mediated effect. Despite weak evidence that they induce great toxicity, a report that also noted a large size-controlled effect mentioned that amorphous TiO_2 NPs did exhibit significantly different toxicity in comparison with those of its anatase and rutile forms (Braydich-Stolle et al., 2009). The abilities of the anatase and rutile NPs to generate RS might be a major reason for their phase-dominated toxicity effects (Sayes et al., 2006); the authors of that study concluded that the anatase phase could induce more RS, but there remains a need to further assess the ability of the amorphous phase to produce RS.

Nano-ZnO and nano-TiO_2 are both inorganic NPs that have significantly different cytotoxicity levels, as measured in this study and also in several other reports (Lin et al., 2009; Yang et al., 2009). Both materials generate ROS (Hussain et al., 2009), but nano-ZnO might also release zinc ions into the cell culture medium, potentially resulting in greater cell damage. Moreover, NPs with positive charge usually penetrate cells more readily than do negatively charged NPs (Harush-Frenkel et al., 2008; Osaka et al., 2009), suggesting that nano-ZnO [zero point of charge (ZPC): ca. 9.3] has greater potential to enter cells and subsequently harm them relative to nano-TiO_2 (ZPC: ca. 6.5). Thus, the chemical composition of an NP is a major influence on its cytotoxicity.

4. Conclusion

NPs of different chemical compositions and properties follow different uptake pathways and employ different mechanisms toward their final biological responses. For this reason, scientists cannot determine the entire toxicity profile merely by studying a single type of NP. In this study, we used self-synthesized NPs, which provided us with shape- and size-controlled nanopowders, to perform in vitro toxicity tests. Both the shape and size of a ZnO NP influence the mitochondria activity and chemokine production of A549 cells. The SSA was an impact factor contributing to the ZnO NPs' cytotoxicity, with the real surface area—through which the particles contacted the internal cells—greatly affecting their toxicity. Furthermore, the crystal structure of nano-TiO_2 influenced its cytotoxicity for a given shape, size, and surface area. We hope that our findings provide a good starting point for future assessments of NP toxicity.

Acknowledgments

We thank the National Science Council (NSC) of the ROC for funding this study and Professors Chien-Hou Wu and Chun-Yu Chuang, Department of Biomedical Engineering and Environmental Sciences, National Tsing-Hua Unversity, for their help with the Zetasizer and biological experiments.

Appendix A. Supplementary data

Supplementary materials related to this article can be found online at doi:10.1016/j.scitotenv.2010.12.033.

References

Adams LK, Lyon DY, Alvarez PJJ. Comparative eco-toxicity of nanoscale TiO_2, SiO_2, and ZnO water suspensions. Water Res 2006;40:3527–32.
Allouni ZE, Cimpan MR, Hol PJ, Skodvin T, Gjerdet NR. Agglomeration and sedimentation of TiO_2 nanoparticles in cell culture medium. Colloid Surf B Biointerfaces 2009;68:83–7.
Aruoja V, Dubourguier HC, Kasemets K, Kahru A. Toxicity of nanoparticles of CuO, ZnO and TiO_2 to microalgae *Pseudokirchneriella subcapitata*. Sci Total Environ 2009;407:1461–8.
Beutler B, Greenwald D, Hulmes JD, Chang M, Pan YC, Mathison J, et al. Identity of tumour necrosis factor and the macrophage-secreted factor cachectin. Nature 1985;316:552–4.
Birchall JD, Stanley DR, Pigott GH, Pinto PJ. Toxicity of silicon carbide whiskers. J Mater Sci Lett 1988;7:350–2.
Braydich-Stolle LK, Schaeublin NM, Murdock RC, Jiang J, Biswas P, Schlager JJ, et al. Crystal structure mediates mode of cell death in TiO_2 nanotoxicity. J Nanopart Res 2009;11:1361–74.
Brown SC, Kamal M, Nasreen N, Baumuratov A, Sharma P, Antony VB, et al. Influence of shape, adhesion and simulated lung mechanics on amorphous silica nanoparticle toxicity. Adv Powder Technol 2007;18:69–79.
Brunauer S, Emmett PH, Teller E. Adsorption of gases in multimolecular layers. J Am Chem Soc 1938;60:309–19.
Brunner TJ, Wick P, Manser P, Spohn P, Grass RN, Limbach LK, et al. In vitro cytotoxicity of oxide nanoparticles: comparison to asbestos, silica, and effects of particle solubility. Environ Sci Technol 2006;44:4373–81.
Cao HL, Qian XF, Gong QQ, Du WM, Ma XD, Zhu ZK. Shape- and size-controlled synthesis of nanometre ZnO from a simple solution route at room temperature. Nanotechnology 2006;17:3632–6.
Carlson C, Hussain SM, Schrand AM, Braydich-Stolle LK, Hess KL, Jones RL, et al. Unique cellular interaction of silver nanoparticles: size-dependent generation of reactive oxygen species. J Phys Chem B 2008;112:13,608–19.
Deng XY, Luan QX, Chen WT, Wang YL, Jiao Z. Nanosized zinc oxide particles induce neural stem cell apoptosis. Nanotechnology 2009;20:115101.
Du HC, Yuan FL, Huang SL, Li JL, Zhu YF. A new reaction to ZnO nanoparticles. Chem Lett 2004;33:770–1.
Ge MY, Wu HP, Niu L, Liu JF, Chen SY, Shen PY, et al. Nanostructured ZnO: from monodisperse nanoparticles to nanorods. J Cryst Growth 2007;305:162–6.
Gojova A, Guo B, Kota RS, Rutledge JC, Kennedy IM, Barakat AI. Induction of inflammation in vascular endothelial cells by metal oxide nanoparticles: effect of particle composition. Environ Health Perspect 2007;115:403–9.
Harush-Frenkel O, Rozentur E, Benita S, Altschuler Y. Surface charge of nanoparticles determines their endocytic and transcytotic pathway in polarized MDCK cells. Biomacromolecules 2008;9:435–43.
Hussain S, Boland S, Baeza-Squiban A, Hamel R, Thomassen LCJ, Martens JA, et al. Oxidative stress and proinflammatory effects of carbon black and titanium dioxide nanoparticles: role of particle surface area and internalized amount. Toxicology 2009;260:142–9.
Ito S, Chen P, Comte P, Nazeeruddin MK, Liska P, Pechy P, et al. Fabrication of screen-printing pastes from TiO_2 powders for dye-sensitised solar cells. Prog Photovoltaics 2007;15:603–12.
Jiang J, Oberdorster G, Elder A, Gelein R, Mercer P, Biswas P. Does nanoparticle activity depend upon size and crystal phase? Nanotoxicology 2008;2:33–42.
Karakoti AS, Hench LL, Seal S. The potential toxicity of nanomaterials—the role of surfaces. JOM 2006;58:77–82.
Karlsson HL, Gustafsson J, Cronholm P, Moller L. Size-dependent toxicity of metal oxide particles—a comparison between nano- and micrometer size. Toxicol Lett 2009;188:112–8.
Kato H, Suzuki M, Fujita K, Horie M, Endoh S, Yoshida Y, et al. Reliable size determination of nanoparticles using dynamic light scattering method for in vitro toxicology assessment. Toxicol In Vitro 2009;23:927–34.
Klug H, Alexander L. X-ray diffraction methods for polycrystalline and amorphous materials. New York: John Wiley and Sons; 1954.
Lam CW, James JT, McCluskey R, Hunter RL. Pulmonary toxicity of single-wall carbon nanotubes in mice 7 and 90 days after intratracheal instillation. Toxicol Sci 2004;77:126–34.
Liao MH, Hsu CH, Chen DH. Preparation and properties of amorphous titania-coated zinc oxide nanoparticles. J Solid State Chem 2006;179:2020–6.
Lin WS, Xu Y, Huang CC, Ma YF, Shannon KB, Chen DR, et al. Toxicity of nano- and micro-sized ZnO particles in human lung epithelial cells. J Nanopart Res 2009;11:25–39.
Malvern Instruments, Ltd. Zetasizer nano series user manual MAN0317 Issue 1.1. UK: Worcestershire; 2004.
Mossman T. Rapid colorimetric assay for cellular growth and survival: application to proliferation and cytotoxicity assays. J Immunol Meth 1983;65:55–63.
Murdock RC, Braydich-Stolle L, Schrand AM, Schlager JJ, Hussain SM. Characterization of nanomaterial dispersion in solution prior to in vitro exposure using dynamic light scattering technique. Toxicol Sci 2008;101:239–53.
Nair S, Sasidharan A, Divya Rani VV, Menon D, Nair S, Manzoor K, et al. Role of size scale of ZnO nanoparticles and microparticles on toxicity toward bacteria and osteoblast cancer cells. J Mater Sci Mater Med 2008;20:235–41.
Napierska D, Thomassen LCJ, Rabolli V, Lison D, Gonzalez L, Kirsch-Volders M, et al. Size-dependent cytotoxicity of monodisperse silica nanoparticles in human endothelial cells. Small 2009;5:846–53.
Nel A, Xia T, Madler L, Li N. Toxic potential of materials at the nanolevel. Science 2006;311:622–7.
Oberdorster G, Oberdorster E, Oberdorster J. Nanotoxicology: an emerging discipline evolving from studies of ultrafine particles. Environ Health Perspect 2005;113:823–39.

Osaka T, Nakanishi T, Shanmugam S, Takahama S, Zhang H. Effect of surface charge of magnetite nanoparticles on their internalization into breast cancer and umbilical vein endothelial cells. Colloid Surf B Biointerfaces 2009;71:325–30.

Pauluhn J. Pulmonary toxicity and fate of agglomerated 10 and 40 nm aluminum oxyhydroxides following 4-week inhalation exposure of rats: toxic effects are determined by agglomerated, not primary particle size. Toxicol Sci 2009;109: 152–67.

Peto J, Doll R, Howard SV, Kinlen LJ, Lewinsohn HC. A mortality study among workers in an English asbestos factory. Brit J Ind Med 1977;34:169–73.

Powers K, Brown S, Krishna V, Wasdo S, Moudgil B, Roberts S. Research strategies for safety evaluation of nanomaterials. Part VI. Characterization of nanoscale particles for toxicological evaluation. Toxicol Sci 2006;90:296–303.

Rejeski D. Nanotechnology and consumer products. Project on Emerging Nanotechnologies: Woodrow Wilson International Center for Scholars; 2009.

Sayes MC, Wahi R, Kurian PA, Liu Y, West JL, Ausman KD, et al. Correlating nanoscale titania structure with toxicity: a cytotoxicity and inflammatory response study with human dermal fibroblasts and human lung epithelial cells. Toxicol Sci 2006;92:174–85.

Sager TM, Kommineni C, Castranova V. Pulmonary response to intratracheal instillation of ultrafine versus fine titanium dioxide: role of particle surface area. Part Fibre Toxicol 2008;5:17.

Sharma V, Shukla RK, Saxena N, Parmar D, Das M, Dhawan A. DNA damaging potential of zinc oxide nanoparticles in human epidermal cells. Toxicol Lett 2009;185: 211–8.

Sun B, Smirniotis PG. Interaction of anatase and rutile TiO_2 particles in aqueous photooxidation. Catal Today 2003;88:49–59.

Warheit DB, Webb TR, Sayes CM, Colvin VL, Reed KL. Pulmonary instillation studies with nanoscale TiO_2 rods and dots in rats: toxicity is not dependent upon particle size and surface area. Toxicol Sci 2006;91:227–36.

Xia T, Kovochich M, Nel AE. Impairment of mitochondrial function by particulate matter (PM) and their toxic components: implications for PM-induced cardiovascular and lung disease. Front Biosci 2007;12:1238–46.

Xia T, Kovochich M, Liong M, Madler L, Gilbert B, Shi H, et al. Comparison of the mechanism of toxicity of zinc oxide and cerium oxide nanoparticles based on dissolution and oxidative stress properties. ACS Nano 2008;2:2121–34.

Yamamoto A, Honma R, Sumita M, Hanawa T. Cytotoxicity evaluation of ceramic particles of different sizes and shapes. J Biomed Mater Res A 2004;68A:244–56.

Yang H, Liu C, Yang DF, Zhang HS, Xi ZG. Comparative study of cytotoxicity, oxidative stress and genotoxicity induced by four typical nanomaterials: the role of particle size, shape and composition. J Appl Toxicol 2009;29:69–78.

Zhang LW, Monteiro-Riviere NA. Mechanisms of quantum dot nanoparticle cellular uptake. Toxicol Sci 2009;110:138–55.